BRAIN
ORIGINAL ARTICLE

Intrinsic blood–brain barrier dysfunction contributes to multiple sclerosis pathogenesis

Hideaki Nishihara,[1,†] Sylvain Perriot,[2] Benjamin D. Gastfriend,[3] Marel Steinfort,[1] Celine Cibien,[1] Sasha Soldati,[1] Kinya Matsuo,[1] Sarah Guimbal,[1] Amandine Mathias,[2] Sean P. Palecek,[3] Eric V. Shusta,[3,4] Renaud Du Pasquier[2] and Britta Engelhardt[1]

Blood–brain barrier (BBB) breakdown and immune cell infiltration into the CNS are early hallmarks of multiple sclerosis (MS). The mechanisms leading to BBB dysfunction are incompletely understood and generally thought to be a consequence of neuroinflammation.

Here, we have challenged this view and asked if intrinsic alterations in the BBB of MS patients contribute to MS pathogenesis. To this end, we made use of human induced pluripotent stem cells derived from healthy controls and MS patients and differentiated them into brain microvascular endothelial cell (BMEC)-like cells as *in vitro* model of the BBB. MS-derived BMEC-like cells showed impaired junctional integrity, barrier properties and efflux pump activity when compared to healthy controls. Also, MS-derived BMEC-like cells displayed an inflammatory phenotype with increased adhesion molecule expression and immune cell interactions. Activation of Wnt/β-catenin signalling in MS-derived endothelial progenitor cells enhanced barrier characteristics and reduced the inflammatory phenotype.

Our study provides evidence for an intrinsic impairment of BBB function in MS patients that can be modelled *in vitro*. Human iPSC-derived BMEC-like cells are thus suitable to explore the molecular underpinnings of BBB dysfunction in MS and will assist in the identification of potential novel therapeutic targets for BBB stabilization.

1 Theodor Kocher Institute, University of Bern, 3012 Bern, Switzerland
2 Laboratory of Neuroimmunology, Lausanne University Hospital (CHUV) and University of Lausanne, Lausanne, Switzerland
3 Department of Chemical and Biological Engineering, University of Wisconsin-Madison, Madison, WI, USA
4 Department of Neurological Surgery, University of Wisconsin-Madison, Madison, WI, USA

† **Present address: Department of Neurotherapeutics, Yamaguchi University, Yamaguchi, Japan**

Correspondence to: Prof. Dr Britta Engelhardt
Theodor Kocher Institute, University of Bern
Freiestrasse 1, 3012 Bern, Switzerland
E-mail: bengel@tki.unibe.ch

Correspondence may also be addressed to: Dr Hideaki Nishihara
E-mail: hidehara@yamaguchi-u.ac.jp

Keywords: multiple sclerosis; blood–brain barrier; human induced pluripotent stem cells; immune cell migration; permeability

Received July 11, 2021. Revised December 17, 2021. Accepted December 20, 2021. Advance access publication January 27, 2022

Introduction

Multiple sclerosis (MS) is considered an autoimmune disorder affecting the CNS, which is caused by the interplay of environmental risk factors and a complex genetic background with now more than 230 quantitative trait loci characterized in genome-wide association studies (GWAS) based on single nucleotide polymorphisms (SNPs).[1,2] MS currently affects 2.3 million people worldwide, but as the aetiology remains unknown, there is no curative treatment available.[3] Although targeting immune cell trafficking across the blood–brain barrier (BBB), or even depleting immune cell subsets, showed remarkable efficacy for preventing relapses, these therapies are associated with side effects including progressive multifoca leukoencephalopathy and show limited impact on the progressive disease phase. It is widely accepted that immune cell trafficking into the CNS and focal breakdown of the endothelial BBB are initial hallmarks of MS pathogenesis. Focal BBB dysfunction is visualized by gadolinium-enhanced MRI and occurs early in the pathogenesis of new lesions in MS.[4] Serial MRI studies have indicated that BBB dysfunction may even precede CNS immune cell infiltration and myelin damage in MS.[5–7] Histopathological studies on post-mortem MS brain tissues have provided evidence for continued abnormalities in BBB function during the progressive phase of MS[8–12] underscoring a central role of BBB dysfunction during the entire course of MS.

Current knowledge about the molecular mechanisms mediating BBB dysfunction in MS have to a large degree been derived from animal models, experimental autoimmune encephalomyelitis (EAE), or autopsy and rare biopsy cases of MS brain samples. Post-mortem brain tissue from MS patients displayed reduced or interrupted staining of tight junction and adherens junction proteins like occludin, claudin-5 and VE-cadherin.[8–12] This picture is associated with fibrinogen and IgG staining outside of blood vessels underscoring the leakage of these serum components across an impaired BBB.[13] Immunostaining for the important efflux pump, P-glycoprotein (P-gp) is also reduced in MS lesions and the function of endothelial P-gp is impaired in EAE.[14] During MS, the endothelial cells of the BBB change their immune phenotype by upregulating intercellular adhesion molecule-1 (ICAM-1), vascular cell adhesion molecule-1 (VCAM-1) and atypical chemokine receptor 1 (ACKR1) in MS lesions[11,12,15–17] allowing for the infiltration of increased numbers of immune cells into the CNS.

However, how these observed BBB alterations precisely contribute to MS pathogenesis, if they are causative or a consequence of CNS inflammation, and what the molecular underpinnings are leading to BBB dysfunction in MS remain unknown. Interestingly first studies performed in animal models have suggested that brain endothelial dysfunction can contribute to the initiation of MS lesion pathogenesis.[18]

Investigating BBB dysfunction in MS is hampered by the fact that BBB samples from MS brains are not readily accessible for research. While CNS biopsies in the early phase of MS are only performed in atypical cases and may thus not reflect typical MS pathogenesis, autopsy material from the progressive stage of MS mainly reflects the advanced stage of the disease.

Recent advancements in stem cell technology have now allowed derivation of human brain microvascular endothelial cell (BMEC)-like cells from human induced pluripotent stem cells (hiPSCs).[19–21] In particular, patient-sourced hiPSC-derived BMEC-like cells uniquely enable the study of BBB dysfunction by providing a scalable and renewable source of BMEC-like cells. Human iPSC-derived *in vitro* models of the BBB have been established[19–23] and proven successful to model BBB dysfunction *in vitro* in inheritable neurological disorders.[24–28]

Since hiPSC-derived CNS cells such as neurons, astrocytes, or oligodendrocytes have proven useful to study MS pathogenesis,[29–37] we here hypothesized that hiPSC-derived *in vitro* BBB models from MS patients may be useful to understand if intrinsic alterations in BBB function contribute to MS pathogenesis. To this end, we established hiPSCs from MS patients and from healthy controls (HC) and differentiated them into BMEC-like cells using two different methodologies, the defined medium method (DMM)[23] and extended endothelial cell culture method (EECM).[20] All MS-patient derived BMEC-like cells showed impaired barrier properties and an increased inflammatory phenotype. Activating Wnt/β-catenin signalling restored BBB properties in MS patient-derived BMEC-like cells. Overall, hiPSC-derived BMEC-like cells are thus suitable to model underlying BBB dysfunction in MS and will assist in the identification of potential novel therapeutic targets for BBB stabilization that may be beneficial for treating early and progressive MS.

Materials and methods

Donors and human induced pluripotent stem cells

Three HC (age/sex: Control HC1 27/F, Control HC2 50/M, Control HC3 49/F) and four patients with relapsing-remitting MS (RR-MS) (age/sex: Patient MS1 15/M, Patient MS2 17/F, Patient MS3 21/F, Patient MS4 31/F) patients were enrolled in this study. The blood of all four MS patients, used for hiPSC differentiation, was drawn at the time of their first relapse, prior to starting disease-modifying treatment (DMT). Subsequently all four MS patients were confirmed to suffer from RR-MS and three of them were put on DMT with natalizumab (Patient MS1) or fingolimod (Patient MS2) or dimethyl fumarate (Patient MS3). hiPSCs were reprogrammed, expanded and characterized for pluripotency and differentiation capacity exactly as described before.[32] To this end the hiPSC quality has been rigorously assessed according to current good laboratory practice in the field set by an international consortia for clinical use of hiPSCs.[38] The testing workflow includes assessment of morphology, karyotyping, exclusion of mycoplasma contamination, pluripotency, capability of differentiation and absence of transgenes (episomes). Each cell line passed all these quality criteria and thus ensures that none of the hiPSCs used in this study presented pre-existing aberrations that would bias the results of the study. Six hiPSC clones from three healthy controls (two clones from each donor) and seven hiPSC clones from four MS patients (two clones from Patients MS1, MS3 and MS4, one clone from Patient MS2) were used in this study.

Human Th1* cells for allogeneic T-cell interaction with EECM-BMEC-like cells

Human $CD4^+$ T cells were isolated, expanded, and sorted as described in previous studies.[39–41] Human Th1* cells were sorted according to their specific expression pattern of chemokine receptors ($CXCR3^+CCR4^-CCR6^+$) from the buffy coat from blood bank. T cells were thawed 1 day prior to the respective experiment and labelled with 1 μM CellTracker™ Green (CMFDA Dye, Life technologies) at 37°C (5% CO_2) for 30 min at the day of the experiment. After labelling, T cells were washed and dead cells were removed by Ficoll-Hypaque gradient (780 g, 20 min, 20°C). T cells were washed twice and resuspended in migration assay medium [Dulbecco's modified Eagle medium (DMEM), 5% foetal bovine

serum (FBS), 4 mM L-Glutamine, 25 mM HEPES] in the appropriate concentration.

Peripheral blood mononuclear cells for autologous immune cell interaction with EECM-BMEC-like cells

Donors Control HC2 and Patient MS3 underwent a leukapheresis (consent form 107/13) in the scope to obtain peripheral blood mononuclear cells (PBMCs). PBMCs were isolated from Control HC2 and Patient MS3 by density gradient centrifugation on Ficoll-Hypaque as described previously[42] and frozen until use. Due to standard clinical procedure, all three included MS patients who were treatment naïve at the time of the initial blood draw (performed to make hiPSC), were put on treatment shortly afterwards and thus under treatment at the time when PBMCs were isolated for this study. Patient MS1 was under natalizumab treatment and excluded as natalizumab specifically blocks lymphocyte binding to the BBB. Patient MS2 was under fingolimod treatment which prohibited isolating sufficient PBMCs from this patients. We therefore isolated PBMCs from Patient MS3 when she was under dimethyl fumarate treatment and showed no clinical activity for more than 3 years.

Differentiation of human induced pluripotent stem cells into BMEC-like cells

The previously published DMM[23] and EECM[20,43] were used to differentiate BMEC-like cells from hiPSCs. To ensure differentiation of hiPSCs to BMEC-like cells in a reproducible manner forming a confluent monolayer with good barrier properties the seeding density for each hiPSC clone was optimized at this step as described.[20,43] For DMM, *hiPSC* seeding densities at Day −3 or Day −4 were optimized at a density between 35 000/cm^2 to 84 000/cm^2 depending on donor and passage (Supplementary Table 1), in order to obtain reproducible differentiation of DMM-BMEC-like cells forming monolayers with excellent barrier properties as determined by high transendothelial electrical resistance (TEER: >2000 Ω × cm^2) and low permeability to sodium fluorescein (NaFl, 376.3 Da: Pe NaFl <0.6 × 10^{-4} cm/min). Accordingly, for EECM, *hiPSC* seeding densities at Day −3 were optimized to a density between 21 000/cm^2 to 100 000/cm^2 depending on donor and passage in order to obtain a high number of endothelial progenitor cells (EPCs) (Supplementary Table 1). EECM-BMEC-like cells at passages between 3–6 were used for assays at Day 6 after seeding onto Transwell® filter inserts at a constant seeding density of 1.12 × 10^5 cells/500 µl. For co-culture with hiPSC-derived smooth muscle like cells (SMLCs), SMLCs and conditioned medium (CM) from SMLCs were obtained as described before.[20,43] TEER was measured using a Volt-Ohm-Meter (Millicell ERS-2, MERSSTX01-electrode). In order to calculate the net resistance in Ω × cm^2 of the cell monolayers, TEER value of an empty filter was subtracted from each measurement and TEER values in Ω were multiplied by the surface area of the filters (1.12 cm²) as follows: TEER (Ω × cm^2) = (cell monolayer resistance—empty Transwell® filter resistance) × surface area (cm^2).

Activation of the Wnt/β-catenin signalling pathway in endothelial progenitor cells

Glycogen synthase kinase-3 (GSK-3) inhibitor, CHIR99021 was used as a Wnt/β-catenin pathway activator. Directly after purification by magnetic activated cell sorting, EPCs were treated with 4 µM CHIR99021 or DMSO as control in hECSR medium until passage 3 (See section 'Activation of Wnt/β-catenin signalling restores barrier properties of MS-derived EECM-BMEC-like cells'. Passage 3 EECM-BMEC-like cells were seeded onto Transwell® filters and used for permeability assays or adhesion molecule phenotyping as described below.

Permeability assay

Permeability of EC monolayers was assessed by measuring the clearance of sodium fluorescein (NaFl, 376.3 Da, Sigma-Aldrich) as previously described.[20,22,43] Briefly, NaFl was added to the upper compartment of the Transwell® inserts at a concentration of 10 µM. Medium samples containing fluorescent tracer that had diffused across the monolayers were collected from the bottom well every 15 min for a total of 60 min, and fluorescence intensity was measured in a Tecan Infinite M1000 multi-well reader (Tecan Trading AG). The experiments were done in triplicates for each condition.

P-glycoprotein function assay: Rhodamine-123 accumulation assays

P-glycoprotein (P-gp) function was assessed by measuring intracellular accumulation of the P-gp substrate Rhodamine 123 in the presence or absence of the P-gp-specific inhibitor cyclosporin A (CsA) as described before.[22] In brief, at Day 8 DMM-BMEC-like cells were seeded onto Matrigel®-coated 24-well plates at a density of 130 000/cm^2. At Day 10, cells were washed with prewarmed Hanks' Balanced Salt Solution (HBSS) and pre-incubated with 10 µM CsA (Sigma C1832) diluted in HBSS or not for 1 h at 37°C (5% CO_2). Then DMM-BMEC-like cells were incubated with Rhodamine 123 (Sigma 83702) in the presence or absence of CsA for 2 h at 37°C (5% CO_2). After two washes with cold PBS, DMM-BMEC-like cells were lysed with RIPA buffer (Sigma R0278). Intracellular accumulation of the fluorescent Rhodamine 123 was measured using a Tecan plate reader (Infinite M1000). Protein concentrations were measured using a BCA protein assay kit (ThermoFisher Scientific) and Rhodamine 123 fluorescence was normalized to protein concentration for each sample. Per cent fold change was calculated by comparing the accumulation of Rhodamine 123 in the absence of the P-gp inhibitor CsA of the same cells in parallel.

Investigation of cell surface expression of adhesion molecules by flow cytometry

Cell surface expression of adhesion molecules was investigated as previously described.[20,43,44] BMEC-like cells differentiated by DMM, or EECM were cultured on Transwell® filter inserts in respective media. Some wells were stimulated with 10 ng/ml of recombinant human TNF-α (R&D systems, 210TA) and 200 IU/ml recombinant human IFN-γ (R&D systems, 285IF) for DMM-BMEC-like cells, and 1 ng/ml of recombinant human TNF-α (R&D systems, 210TA) and 20 IU/ml recombinant human IFN-γ (R&D systems, 285IF) for EECM-BMEC-like cells for 16 h at 37°C (5% CO_2). Detailed information about antibodies is listed in Supplementary Table 2.

Immunofluorescence stainings and cell size calculation

BMEC-like cells differentiated by DMM, or EECM were cultured on Transwell® filter inserts as described previously.[20,23,43] To stain for claudin-5, occludin, VE-cadherin, cells were fixed with methanol, blocked and permeabilized with 5% skimmed milk containing 0.1% Triton X-100, and then stained with primary antibodies for

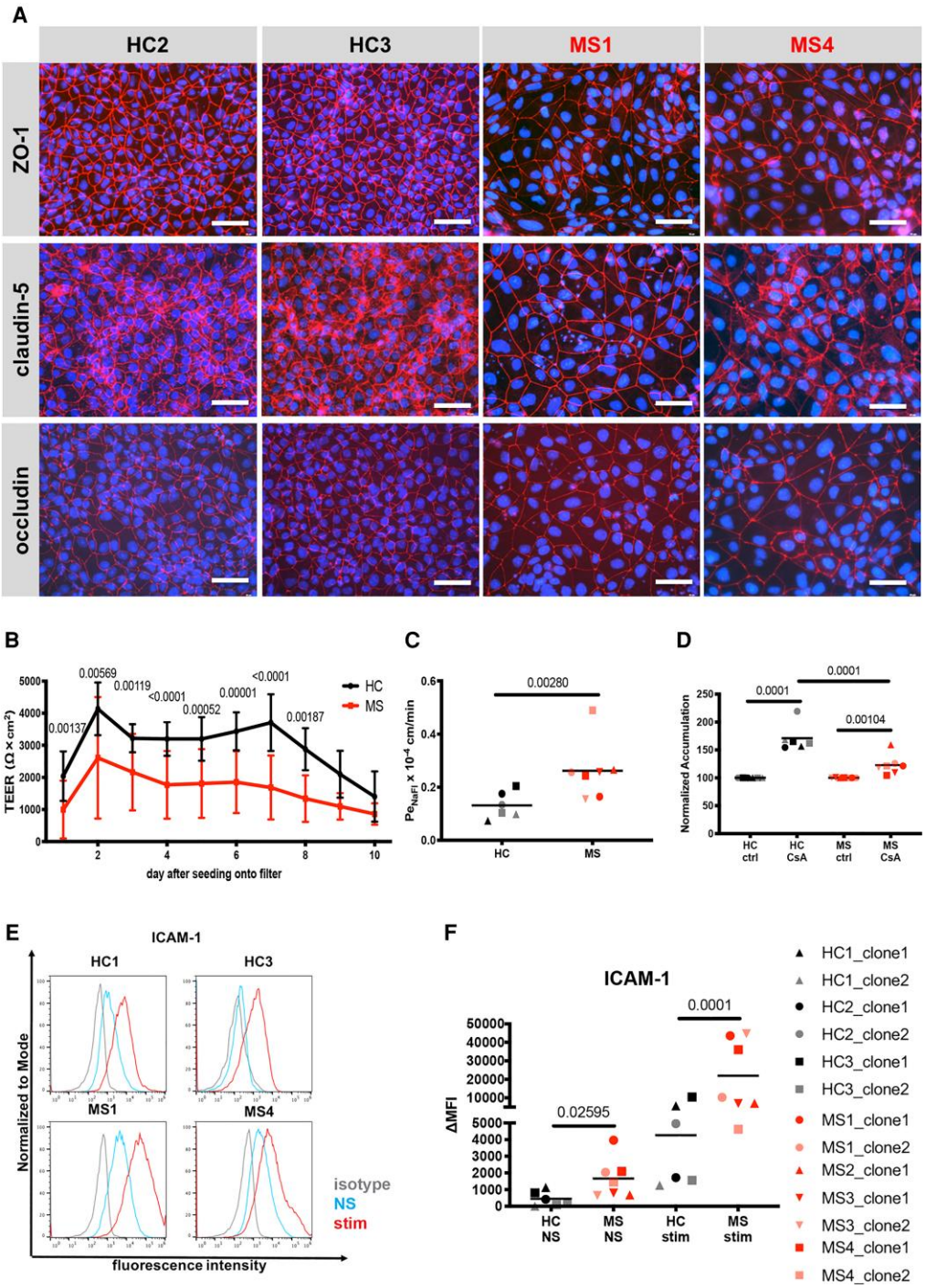

Figure 1 Morphological and functional differences in MS-patient versus HC-derived DMM-BMEC-like cells. (**A**) Representative stainings for ZO-1, claudin-5, or occludin (red), and nuclei (DAPI, blue) from Control HC1, Control HC3, Patient MS1 and Patient MS4 are shown. Each staining is representative of at least three independent experiments using three individual differentiations. Scale bar = 50 μm. (**B**) Transendothelial electrical resistance (TEER) measured with a Volt-Ohm metre. The black line represents mean ± standard deviation (SD) of six clones from three HC and red line represents mean ± SD of seven clones from four MS patients each performed in triplicates and repeated at least twice using two individual differentiations for each donor. (**C**) Permeability of sodium fluorescein (NaFl) across DMM-BMEC-like cell monolayers was measured. (**D**) P-gp efflux pump activity was assessed by intracellular accumulation of Rhodamine 123 in the presence or absence of the P-gp inhibitor cyclosporine A (CsA). (**E**) Cell surface staining for the adhesion molecule ICAM-1 analysed by flow cytometry is shown. Isotype control, non-stimulated (NS) and 16 h pro-inflammatory cytokine-stimulated conditions are shown with the grey, blue and red lines, respectively. Representative data from Controls HC1 and HC3 and Patients MS1 and MS4 are shown from at least two independent differentiations. (**F**) The change in geometric mean (ΔMFI = MFI staining–MFI isotype) of cell surface ICAM-1 as analysed by flow cytometry. (**C**, **D** and **F**) Bars show the mean of six clones from three HC or seven clones from four MS patients. Each symbol (HC: black, MS: red) represents the mean of at least two independent experiments using two individual differentiations each performed in at least triplicates. Statistical analysis was performed as outlined in the 'Materials and methods' section. *P*-values are indicated in the respective figures.

1 h at room temperature as described.[22,23,43,45] After three washes, cells were incubated with respective secondary antibodies for 1 h at room temperature. For staining of cell surface ICAM-1 and VCAM-1, primary antibodies were added to live cells and incubated at 37°C (5% CO_2) for 15 min. After washing, cells were fixed with 1% (w/v) formaldehyde, blocked with 5% skimmed milk and then incubated with secondary antibodies as described.[43,45] Nuclei were stained with DAPI at 1 µg/ml. After washing with DPBS, cell monolayers on filters were mounted with Mowiol (Sigma-Aldrich). Images were acquired using a Nikon Eclipse E600 microscope using the Nikon NIS-Elements BR3.10 software (Nikon). Detailed information about antibodies is listed in Supplementary Table 2.

Average cell numbers and cell sizes per field of view (FOV) were determined using these images of the EECM-BMEC-like cell monolayers stained with DAPI for nuclei and for VE-cadherin, claudin-5 or occludin for endothelial junctions using Fiji image processing. Image noise was reduced by applying the Gaussian Blur filter and separation of overlapping signals was achieved by applying watershed segmentation. The nuclei per FOV were counted using the analyse particles tool of Fiji. The area of each FOV was calculated based on the scale bar included in each image and the mean size of the cells was calculated by dividing the area of each FOV (μm^2) with number of nuclei.

Adhesion assays

Adhesion assays were performed as previously descried.[20,43] EECM-BMEC-like cells were cultured on collagen-IV/fibronectin-coated 16-well chamber slides (ThermoFisher) at a density of 75 000/cm^2 using hECSR medium. Once EECM-BMEC-like cells attached to the chamberslides, hECSR was replaced for SMLC-derived CM from the same clones. EECM-BMEC-like cells were stimulated or not with 0.1 ng/ml TNF-α + 2 IU/ml IFN-γ for 16 h at 37°C (5% CO_2). Th1* cells ($n = 20\,000$) from allogeneic healthy control donors were co-incubated with the EECM-BMEC-like cells monolayers at room temperature for 30 min under slight movement using a rocking platform. Chamber slides were gently washed twice and fixed with 2.5% glutaraldehyde for 2 h on ice. Filters were then washed with DPBS, and adherent fluorescence labelled Th1* cells per pre-defined FOV were analysed by fluorescence microscopy (Nikon Eclipse E600) and FIJI software (Version 2.0.0, Image J, USA). Assays were performed in at least quadruplicates in each condition for each experiment.

In vitro live cell imaging

In vitro live cell imaging of Th1* cell and PBMC interactions with EECM-BMEC-like cells under physiological flow was performed as previously described.[20] Briefly, EECM-BMEC-like cells were cultured in cloning rings placed on collagen IV/fibronectin-coated Ibidi µ-dishes (Ibidi). EECM-BMEC-like cells were stimulated with 0.1 ng/ml recombinant human TNF-α + 2 IU/ml IFN-γ for 16 h at 37°C (5% CO_2) diluted in conditioned medium from SMLC. Fluorescently labelled immune cells were allowed to accumulate on the EECM-BMEC-like cell monolayer at a low flow rate of 0.1 dyne/cm^2 for 4 min, and then the flow rate was set to the physiological level of 1.5 dyne/cm^2 for 16 min (shear phase). The dynamic immune cell interactions with the EECM-BMEC-like cell monolayers under the physiological flow were recorded with a Zeiss Axiocam MRm camera. Immune cell behaviour on the EECM-BMEC-like cell monolayer was categorized as described previously.[45] In brief, Th1* cells and PBMCs found to polarize upon arrest and to migrate across the EECM-BMEC-like cells monolayer with or without prior crawling or probing on the EECM-BMEC-like cells were categorized as 'diapedesis'. Th1* cells and PBMCs that crawled on the surface of the EECM-BMEC-like cells for the entire observation time were categorized as 'crawling'. Th1* cells and PBMCs that remained stationary without displacing beyond a distance exceeding their own diameter and presenting dynamic cellular protrusions were categorized as 'probing'.

Quantitative RT-PCR

RNA was isolated using High Pure RNA isolation kit (Roche) as instructed by the manufacturer, from EECM-BMEC-like cells. For quantitative real time PCR analyses, total RNA was reverse transcribed with Maxima H Minus cDNA Synthesis Master Mix (ThermoFisher Scientific), and amplification was performed on an ABI PRISM 7000 Sequence Detection System (ThermoFisher Scientific) using Takyon ROX SYBR Green MasterMix dTTP Blue (Eutogentec). Primer sequences are reported in Supplementary Table 3. The relative expression of each mRNA was calculated by the comparative threshold cycle method and normalized to β-actin mRNA expression.

Statistical analysis

Statistical analysis of the data was performed by the Clinical Trial Unit (CTU) of the University of Bern. Multiple measurements per clone within each individual were analysed through a linear mixed model. In order to take into account the potential correlation between clones from the same individual, random intercept and slope for clone nested into individual were considered. Robust standard errors were considered for the mixed model. Variances of the random parameters were displayed as well as the intra-class correlation (ICC) between clones. The linear mixed model does not require normal distribution of the data but of the error terms of the model and there is no evidence against non-normality of the errors in our dataset. Importantly, robust standard error is more stable against such deviation and has been considered in our analysis. All analyses were done using Stata version 17. StataCorp. 2021. Stata Statistical Software: Release 17. College Station, TX: StataCorp LLC. *P*-values are indicated in each figure.

Study approval

All subjects have given their written informed consent for establishing hiPSCs [consent form 107/13 and 2018-01622 (Patients MS3 and MS4) and OFSEP consent (Patients MS1 and MS2)] and derivatives thereof according to the ethical approval for the project entitled 'COOLIN' BRAIN' given of the Cantonal Ethic Committee of the Canton Vaud (Switzerland) (consent form 2018-01622).

Data availability

All data are available in the main text or the Supplementary material.

Results

MS-derived DMM-BMEC-like cells show impaired barrier characteristics

To investigate if BMEC-like cells differentiated from hiPSCs of MS patients model BBB dysfunction, we established six hiPSC clones from three healthy controls and seven hiPSC clones from four MS patients and differentiated them into BMEC-like cells by the well established

and widely used DMM.[23] BMEC-like cells derived using the DMM method are particularly useful for the investigation of barrier and transport characteristics of the human BBB, despite their shortcomings in modelling endothelial development and immune cell interactions.[20,46–48] We found that both control- and MS-derived DMM-BMEC-like cells show junctional localization of the tight junction molecules claudin-5 and occludin and the junctional scaffolding protein ZO-1 (Fig. 1A). However, MS-derived DMM-BMEC-like cells were larger in size when compared to control (HC)-derived DMM-BMEC-like cells despite equivalent seeding densities two days prior to analysis (Fig. 1A). When investigating barrier characteristics of DMM-BMEC-like cells by studying the TEER and the permeability to the small molecule tracer NaFl (0.37 kDa), we found that MS-derived DMM-BMEC-like cells showed an accelerated decline of TEER (Fig. 1B) and a significantly higher permeability to NaFl (Fig. 1C) when compared to HC-derived DMM-BMEC-like cells. Thus, MS-derived DMM-BMEC-like cells display a distinct morphology with impaired junctional integrity and barrier characteristics when compared to HC-derived DMM-BMEC-like cells.

MS-derived DMM-BMEC-like cells display reduced P-glycoprotein efflux pump activity

As expression of the efflux pump P-gp is known to be reduced in active MS lesions and P-gp function is impaired in EAE[14] we next asked if any changes in P-gp activity could be detected in MS-derived DMM-BMEC-like cells. To this end, we assessed the accumulation of the P-gp substrate Rhodamine 123 in the presence or absence of the P-gp inhibitor CsA in MS- and HC-derived DMM-BMEC-like cells. While we observed increased accumulation of Rhodamine 123 in both MS- and HC-derived DMM-BMEC-like cells upon CSA treatment, accumulation of Rhodamine 123 was significantly lower in MS-derived DMM-BMEC-like cells compared to HC-derived DMM-BMEC-like cells (Fig. 1D, HC: 172.7 ± 26.63%, MS: 123.7 ± 19.27%), indicating an impaired P-gp function.

MS-derived DMM-BMEC-like cells show increased cell surface staining of ICAM-1

Another key pathological hallmark of MS is increased expression of endothelial adhesion molecules mediating CNS immune cell infiltration. Therefore, we next asked if MS-derived DMM-BMEC-like cells show increased cell surface expression of ICAM-1, which mediates T-cell arrest and crawling on the inflamed BBB.[49] Comparing cell surface expression of ICAM-1 by flow cytometry, we found that both HC- and MS-derived DMM-BMEC-like cells stained positive for ICAM-1, and proinflammatory cytokine stimulation induced further upregulation of ICAM-1. Interestingly, MS-derived DMM-BMEC-like cells showed a significantly higher cell surface ICAM-1 staining under both non-stimulated and proinflammatory cytokine-stimulated conditions compared to HC-derived DMM-BMEC-like cells (Fig. 1E and F). Increased ICAM-1 expression on MS-derived DMM-BMEC-like cells suggests an intrinsic inflammatory phenotype that may contribute to increased immune cell trafficking into the CNS in MS.

EECM-BMEC-like cells from MS patients show disrupted tight junctions and impaired barrier properties

As DMM-BMEC-like cells do not express other key adhesion molecules expressed on the BBB *in vivo*,[20] they are not suited to model BBB-immune cell interactions in MS. We therefore conducted further studies using a complementary hiPSC BBB model known as EECM-BMEC-like cells, which we have previously shown to be suitable to study immune cell interactions with the BBB *in vitro*.[20] Therefore, we differentiated six hiPSC clones from three HCs and seven hiPSC clones from four MS patients into BMEC-like cells by EECM. We first asked whether the observed MS-associated BBB dysfunction modelled by DMM-BMEC-like cells could be reproduced with EECM-BMEC-like cells. We successfully differentiated HC- and MS-derived iPSCs to EECM-BMEC-like cells that showed junctional localization of adherens and tight junction proteins VE-cadherin, claudin-5 and occludin (Fig. 2A). We have previously shown that EECM-BMEC-like cells have a morphology that is distinct from DMM-BMEC-like cells and resembles more that of primary brain microvascular endothelial cells.[20,43] In accordance with observations of DMM-BMEC-like cells, MS-derived EECM-BMEC-like cells were larger in size (Supplementary Fig. 1A) and showed interrupted junctional staining for the tight junction proteins claudin-5 and occludin despite equal seeding density (Fig. 2A). MS-derived EECM-BMEC-like cells established a significantly lower TEER and showed a significantly increased permeability to NaFl when compared to HC-derived EECM-BMEC-like cells (Fig. 2B–D). Importantly, we previously demonstrated that co-culture of EECM-BMEC-like cells with SMLC derived from the same hiPSC clones helped to improve the adhesion molecule repertoire.[20] Co-culture with SMLC increased permeability in both HC and MS-derived EECM-BMEC-like cells, with MS-derived EECM-BMEC-like cells having a similar fold increased in permeability as in the monoculture case. (Fig. 2E). To investigate the possibility that larger morphology, interrupted tight junction proteins and corresponding impairment of barrier properties of MS-derived EECM-BMEC-like cells was caused by a slower proliferation rate, we cultured MS-derived EECM-BMEC-like cells for 8 days (2 days longer) after seeding on the Transwell® filter and evaluated claudin-5 staining by immunocytochemistry. The morphology and interrupted claudin-5 staining of MS-derived EECM-BMEC-like cells were unchanged (Supplementary Fig. 1B). We also investigated the permeability of NaFl in HC- versus MS-derived EECM-BMEC-like cell monolayers at different seeding densities, lower density for HC and higher density for MS. Although HC-derived EECM-BMEC-like cells in monolayers obtained from reduced seeding density displayed a morphology comparable to that of MS-derived EECM-BMEC-like cells at normal density, they sustained continuous junctional localization of claudin-5 and low permeability to NaFl (Supplementary Fig. 1C and D). Also, MS-derived EECM-BMEC-like cell monolayers obtained after increased EECM-BMEC-like cell seeding density did not show any difference in permeability for NaFl when compared to regular seeding density (Supplementary Fig. 1C and D). These results indicate that while cellular morphology is dependent on seeding density, impaired functionality of MS-derived EECM-BMEC-like cells does not depend on seeding densities. Thus, MS-derived EECM-BMEC-like cells show impaired junctional integrity and defective barrier properties suggesting that BBB dysfunction in MS can indeed be modelled with hiPSC-derived EECM-BMEC-like cells.

MS-derived EECM-BMEC-like cells show increased cell surface staining of ICAM-1 and VCAM-1

We next asked if using EECM-BMEC-like cells we could also model increased expression of ICAM-1 and VCAM-1 as observed in brain endothelium of MS patients.[50] To this end, we immunolabelled for endothelial adhesion molecules ICAM-1 and VCAM-1 on EECM-BMEC-like cells co-cultured with SMLCs (Fig. 3A). We found that MS-derived EECM-BMEC-like cells had a qualitatively higher

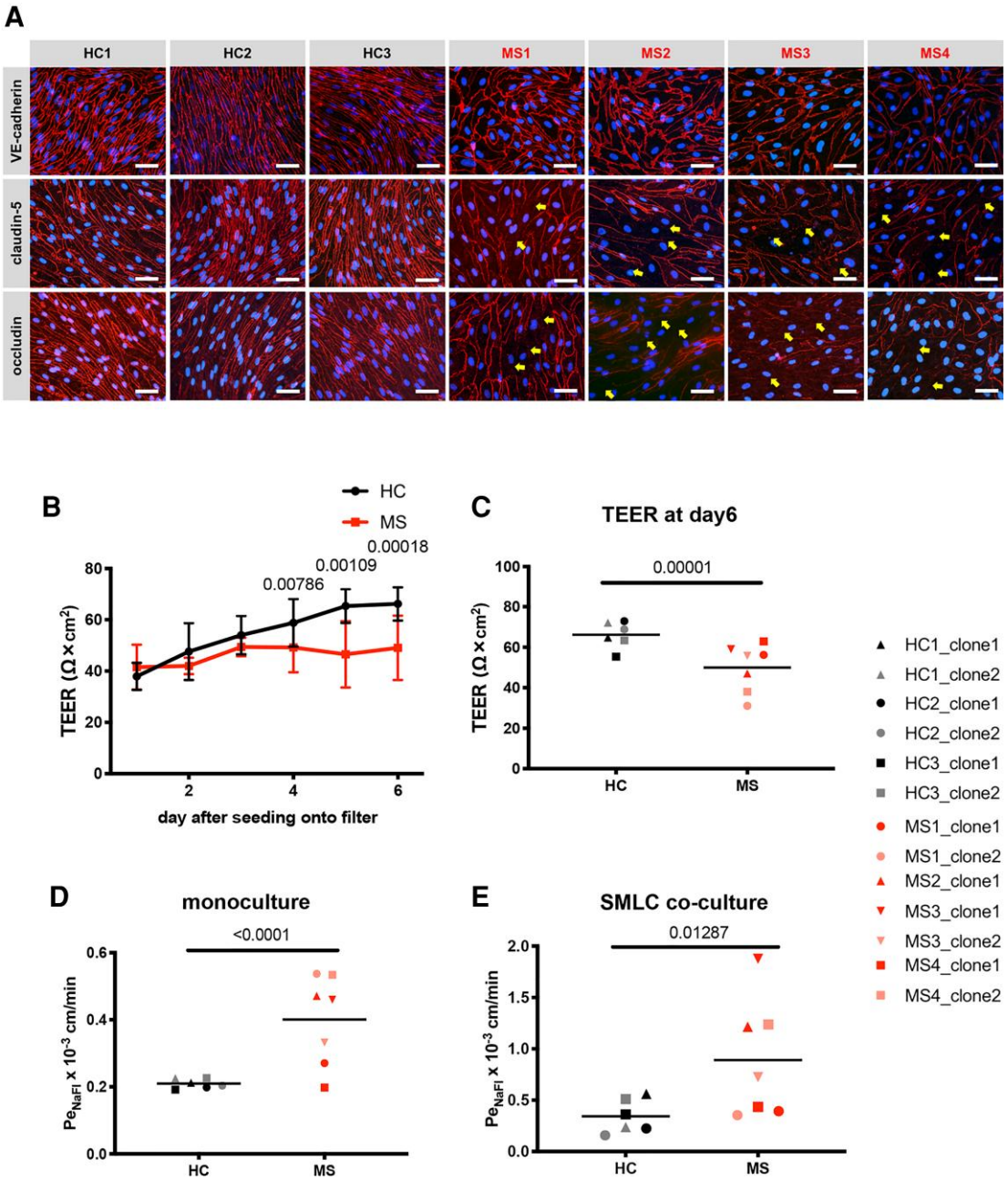

Figure 2 Impaired barrier characteristics in MS- versus HC-derived EECM-BMEC-like cells. (**A**) Immunofluorescence stainings of EECM-BMEC-like cells in co-culture with SMLC for 6 days are shown. Junctions were stained for VE-cadherin, claudin-5, or occludin (red), and nuclei were stained with DAPI (blue). Representative images of three HC and four MS from at least three independent experiments using three individual differentiations performed on three distinct filters are shown. Yellow arrows indicate visible disruptions of junctional stainings for claudin-5 and occludin. Scale bar = 50 μm. (**B**) TEER of EECM-BMEC-like cell monolayers derived from HC versus MS patients is shown. Black line represents mean ± SD of six clones from three HC and red line represents mean ± SD of seven clones from four MS-patients each performed in triplicates and repeated at least twice using two individual differentiations for each donor. (**C**) TEER at Day 6 after seeding onto filters of EECM-BMEC-like cell monolayers derived from HC versus MS is shown. (**D** and **E**) Permeability of NaFl across EECM-BMEC-like cell monolayers: EECM-BMEC-like cells derived from HC (black) or MS patients (red) were cultured to confluency on 0.4 μm pore size Transwell® filters in monoculture (**D**) or co-culture with SMLC from the same donor (**E**) for 6 days and permeability of NaFl was measured at Day 6 after seeding onto the filter. (**C–E**) Bars show the mean of six clones from three HC and seven clones from four MS patients. Each symbol (HC: black, MS: red) shows the mean of at least two independent experiments using two individual differentiations each performed in at least triplicates. Statistical analysis was performed as outlined in the 'Materials and methods' section. *P*-values are indicated in the respective figures.

ICAM-1 signal under both non-stimulated and proinflammatory cytokine-stimulated (1 ng/ml TNF-α + 20 IU/ml IFN-γ) conditions and higher VCAM-1 signal under proinflammatory cytokine-stimulated conditions compared to HC-derived EECM-BMEC-like cells (Fig. 3A). Quantitative flow cytometry analyses of non-stimulated (NS) or proinflammatory cytokine-stimulated EECM-BMEC-like cells confirmed the increased cell surface expression of ICAM-1 and VCAM-1 in MS-derived EECM-BMEC-like cells (Fig. 3B and C). Mean fluorescence intensities for VCAM-1 seemed generally much lower when compared to ICAM-1 (Fig. 3C) and

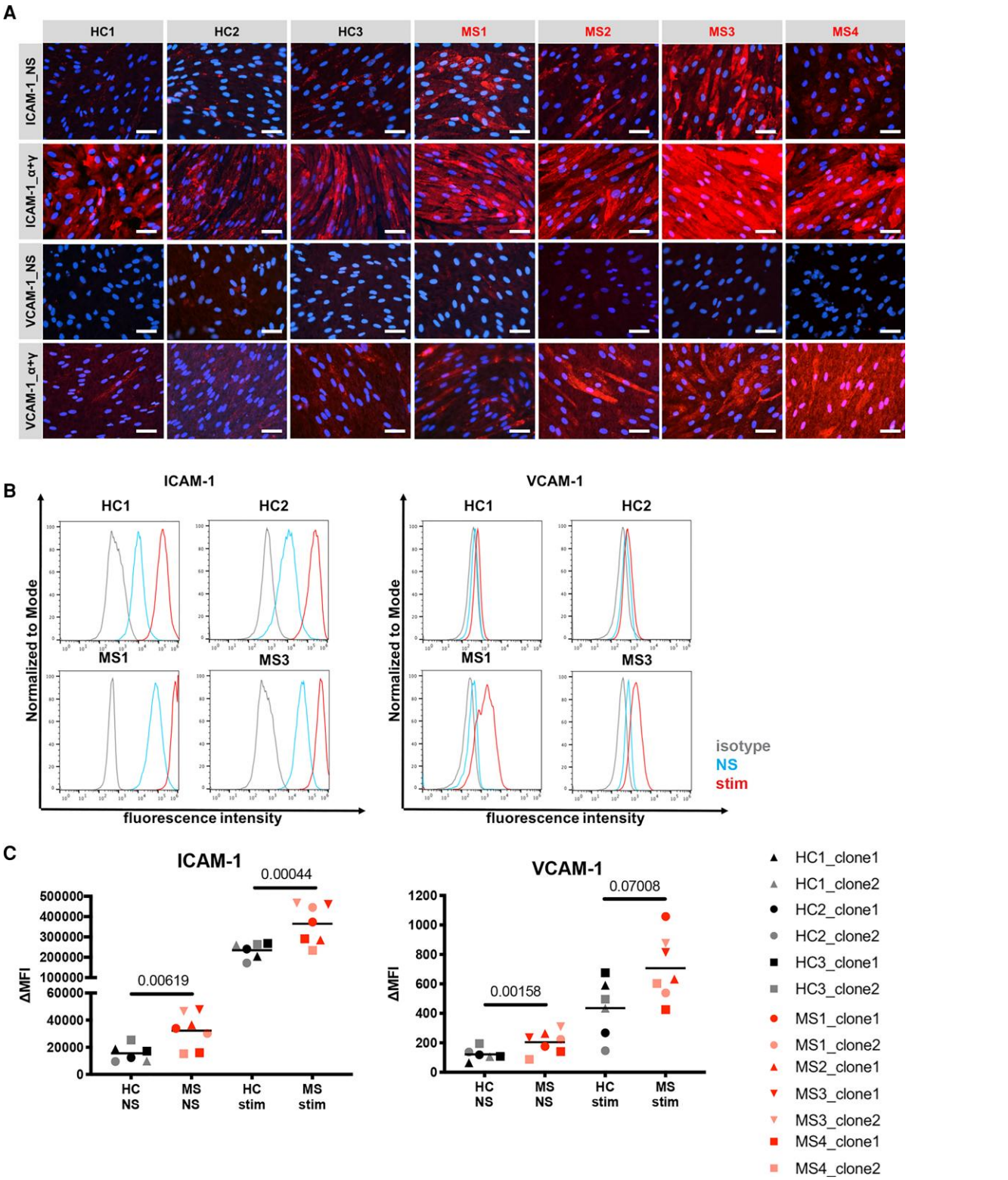

Figure 3 MS-derived EECM-BMEC-like cells show enhanced cell surface expression of ICAM-1 and VCAM-1. (**A**) Immunofluorescence stainings of EECM-BMEC-like cell monolayers for ICAM-1, VCAM-1 (red) are shown. Nuclei were stained with DAPI (blue). Each staining is representative of at least three independent experiments using three individual differentiations performed on three distinct filters. NS and 1 ng/ml TNF-α + 20 IU/ml IFN-γ stimulated conditions are shown. Scale bars = 50 μm. (**B**) Cell surface staining of EECM-BMEC-like cells for the adhesion molecules ICAM-1 and VCAM-1 was analysed by flow cytometry. Isotype control, non-stimulated (NS), and 16 h pro-inflammatory cytokine-stimulated condition are shown in grey, blue, and red lines respectively. Representative data from Controls HC1 and HC2, and Patients MS1 and MS3 are shown. (**C**) The change in geometric mean (ΔMFI = MFI staining–MFI isotype) of cell surface ICAM-1 and VCAM-1 of EECM-BMEC-like cells was analysed by flow cytometry. Each symbol (HC: black, MS: red) represents the mean of at least two experiments using two independent differentiations. Bars show the mean of six clones from three HC and seven clones from four MS. Statistical analysis was performed as outlined in the 'Materials and methods' section. *P*-values are indicated in the respective figures.

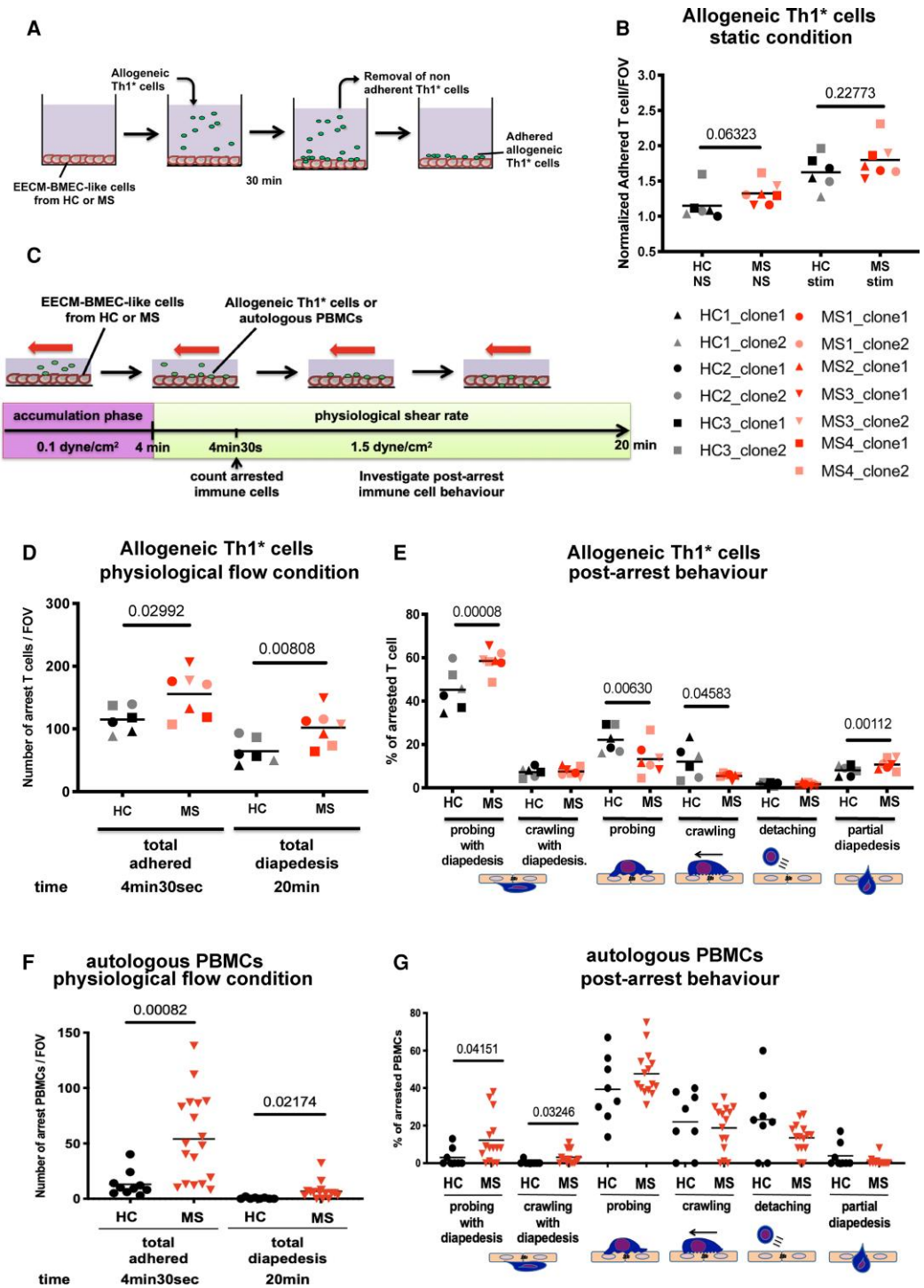

Figure 4 MS-derived EECM-BMEC-like cells support increased immune cells interaction. (**A**) Schematic representation of the adhesion assay. (**B**) The number of allogeneic Th1* cells adherent to NS and pro-inflammatory cytokine-stimulated EECM-BMEC-like cell monolayers derived from HC versus MS patients was counted after 30 min under static conditions. In each assay, Th1* cell adhesion to EECM-BMEC-like cells from HC2 clone1 under NS conditions was included and the number of adherent Th1* cells/FOV was normalized to this condition (Control HC2 clone 1 NS condition = 1). (**C**) Schematic for *in vitro* live cell imaging of immune cell/BMEC interaction under physiological flow. (**D–G**) Analysis of the arrest and post-arrest behaviour of allogeneic Th1* cell or autologous PBMC interactions with pro-inflammatory cytokine-stimulated EECM-BMEC-like cells in the field of view of the videos (example in Supplementary Videos 1 and 2 for allogeneic Th1* and Supplementary Videos 3 and 4 for autologous PBMCs) under physiological flow. (**D** and **F**) The number of allogeneic Th1* cells (**D**) or autologous PBMCs (**F**) remaining arrested on the EECM-BMEC-like cell monolayer were quantified at the end of the accumulation phase at 4 min 30 s. The number of Th1* cells or PBMCs that had migrated across EECM-BMEC-like cells were counted at 20 min. (**E** and **G**) Post-arrest allogeneic Th1* cell (**E**) or autologous PBMCs (**G**) behaviour on the EECM-BMEC-like cell monolayers under flow was analysed. (**F** and **G**) Autologous PBMCs from Control HC2 or Patient MS3 were used in this assay. (**B**, **D–G**) Each symbol (HC: black, MS: red) represents the mean of at least three experiments using two independent differentiations. Bars show the mean of six clones from three HC and seven clones from four MS. Statistical analysis was performed as outlined in the 'Materials and methods' section. *P*-values are indicated in the respective figures.

were accordingly barely detectable by immunofluorescence staining on non-stimulated EECM-BMEC-like cells (Fig. 3A). Finally, when comparing the fold upregulation of ICAM-1 and VCAM-1 after cytokine stimulation, HC-derived and MS-derived EECM-BMEC-like cells did not show any difference (data not shown). Taken together, MS-derived EECM-BMEC-like cells displayed significantly increased expression of ICAM-1 at both basal and cytokine-stimulated conditions and VCAM-1 at basal condition and thus permit modelling of the inflammatory BBB phenotype observed in MS *in vivo*.

MS-derived EECM-BMEC-like cells promote increased adhesion and transmigration of allogeneic Th1* cells

As we have previously shown that ICAM-1 and VCAM-1 on EECM-BMEC like cells mediate T-cell adhesion,[20] we next asked if increased expression of ICAM-1 and VCAM-1 in MS-derived EECM-BMEC-like cells would translate to increased T cell trafficking across their barrier. To this end, we first investigated the interaction of EECM-BMEC-like cells with Th1* cells since this T cell subset is present in CSF and brain parenchyma of MS patients[51,52] and thought to contribute to MS pathogenesis because of its mixed Th1/Th17 signature cytokine profile secreting IFN-γ, IL-17 and GM-CSF.[51–53] Incubating allogeneic Th1* cells isolated from healthy donors with MS-derived and HC-derived EECM-BMEC-like cell monolayers under static conditions (Fig. 4A) we found an increased tendency in adhesion of Th1* cells to MS-derived EECM-BMEC-like cells when compared to HC-derived EECM-BMEC-like cells under non-stimulated but no longer under cytokine-stimulated conditions, when adhesion molecule expression on HC-EECM-BMEC-like cells was further upregulated (Fig. 4B). To determine if increased interaction of Th1* cells with MS-derived EECM-BMEC-like cells would also lead to increased Th1* cell migration across MS-derived EECM-BMEC-like cells, we next investigated the interaction of Th1* cells with EECM-BMEC-like cells under physiological flow by *in vitro* live cell imaging (Fig. 4C). Under these conditions, which better recapitulate the sequential adhesive interactions of the multi-step T-cell extravasation cascade as they occur *in vivo*, we could observe increased shear resistant arrest of allogeneic Th1* cells to cytokine-stimulated MS-derived EECM-BMEC-like cells when compared to HC-derived EECM-BMEC-like cells (Fig. 4D). This ultimately translated into increased Th1* cell diapedesis across MS-derived EECM-BMEC-like cells compared to HC-derived EECM BMEC-like cells (Fig. 4D and Supplementary Videos 1 and 2). Upon shear-resistant arrest, T cells either probe the endothelial cell surface by sending out cellular protrusions or they crawl over the endothelial surface to find sites permissive for diapedesis.[49] The majority of Th1* cells crossed the EECM-BMEC-like cell monolayers after probing while a lower percentage crossed the EECM-BMEC-like cell monolayers after crawling (Fig. 4E). The percentage of arrested Th1* cells that crossed the EECM-BMEC-like cells after probing was significantly higher in MS-derived EECM-BMEC-like cells compared to HC-derived EECM-BMEC-like cells. Conversely, Th1* cell probing or crawling on the EECM-BMEC-like cell surface over the entire assay period without diapedesis was significantly higher on HC-EECM-BMEC-like cells when compared to their MS counterparts suggesting that lower cell surface expression of adhesion molecules on HC-EECM-BMEC-like cells delayed the Th1* cells in finding appropriate sites for diapedesis (Fig. 4E). Taken together, these observations underscore that alterations in MS-derived EECM-BMEC-like cells cause increased T-cell adhesion followed by increased T-cell diapedesis as compared to HC-derived EECM-BMEC-like cells reflecting the observations made *in vivo* in MS.

MS-derived EECM-BMEC-like cells support increased interaction with autologous PBMCs

Having established that MS-derived EECM-BMEC like cells model BBB impairment and an increased inflammatory phenotype as observed in MS *in vivo* we made use of this unprecedented opportunity to study MS-patient derived immune cell interactions with the BBB in an entirely autologous fashion *in vitro*. To this end we obtained PBMCs from Control HC2 and Patient MS3 and compared their interactions side-by-side with Control HC2- and Patient MS3-derived EECM-BMEC like-cells in an autologous or heterologous setting under physiological flow by *in vitro* live cell imaging. Although we showed in a previous study that DMF reduces binding of peripheral blood T cells to the BBB *in vitro*,[54] when comparing the autologous interactions of PBMCs with EECM-BMEC-like cells we here found significantly higher numbers of Patient MS3-derived PBMCs adhering to or crossing Patient MS3-derived EECM-BMEC-like cell monolayers when compared to Control HC2-PBMCs interaction with Control HC2-derived EECM-BMEC-like cells (Fig. 4F). In-depth analysis of the individual post-arrest behaviour of PBMCs on the EECM-BMEC-like cell monolayers showed that in the autologous MS system, there was a trend towards increased diapedesis in both probing and crawling PBMCs accompanied by a trend towards reduced PBMC detachment (Fig. 4G). However, as the composition and activation stage of PBMCs in MS patients differs from that in HCs we next asked if increased interaction of PBMCs with EECM-BMEC-like cells as observed in the autologous MS setting is truly a function of the BMEC-like cells themselves. To this end, we analysed the interaction of Control HC2-derived PBMCs with Patient MS3-derived EECM-BMEC-like cells and Patient MS3-derived PBMCs with Control HC2-derived EECM-BMEC-like cells under physiological flow *in vitro*. Patient MS3-derived EECM-BMEC-like cells supported a significantly increased arrest, crawling and diapedesis of Control HC2-derived PBMCs under physiological flow *in vitro* when compared to the autologous Control HC2-derived EECM-BMEC-like cells (Supplementary Fig. 2A and B). Also, Patient MS3 PBMCs showed a significantly increased arrest and subsequent probing on autologous EECM-BMEC-like cells when compared to Patient HC2-derived EECM-BMEC-like cells (Supplementary Fig. 2C and D). Taken together, these data underscore the inflammatory phenotype and active role of the MS-derived EECM-BMEC-like cells in increasing immune cell entry into the CNS and their suitability to explore immune functions of the BBB in an entirely autologous fashion.

Activation of Wnt/β-catenin signalling restores barrier properties of MS-derived EECM-BMEC-like cells

Having established that MS-derived EECM-BMEC-like cells are suitable to model BBB dysfunction in MS we next explored if this model is appropriate to evaluate therapeutic strategies for the treatment of MS at the level of the BBB. As the canonical Wnt/β-catenin signalling pathway is involved in BBB development and maintenance,[55–57] and we have demonstrated that activation of Wnt/β-catenin signalling upregulates claudin-5 and induced other BBB properties in hPSC-derived generic ECs,[58] we investigated if expression of molecules involved in canonical Wnt/β-catenin signalling is modulated in MS-derived EECM-BMEC-like cells. To this end we performed RT-qPCR experiments (Supplementary Fig. 3A–E). While *FZD3*, *FZD4*

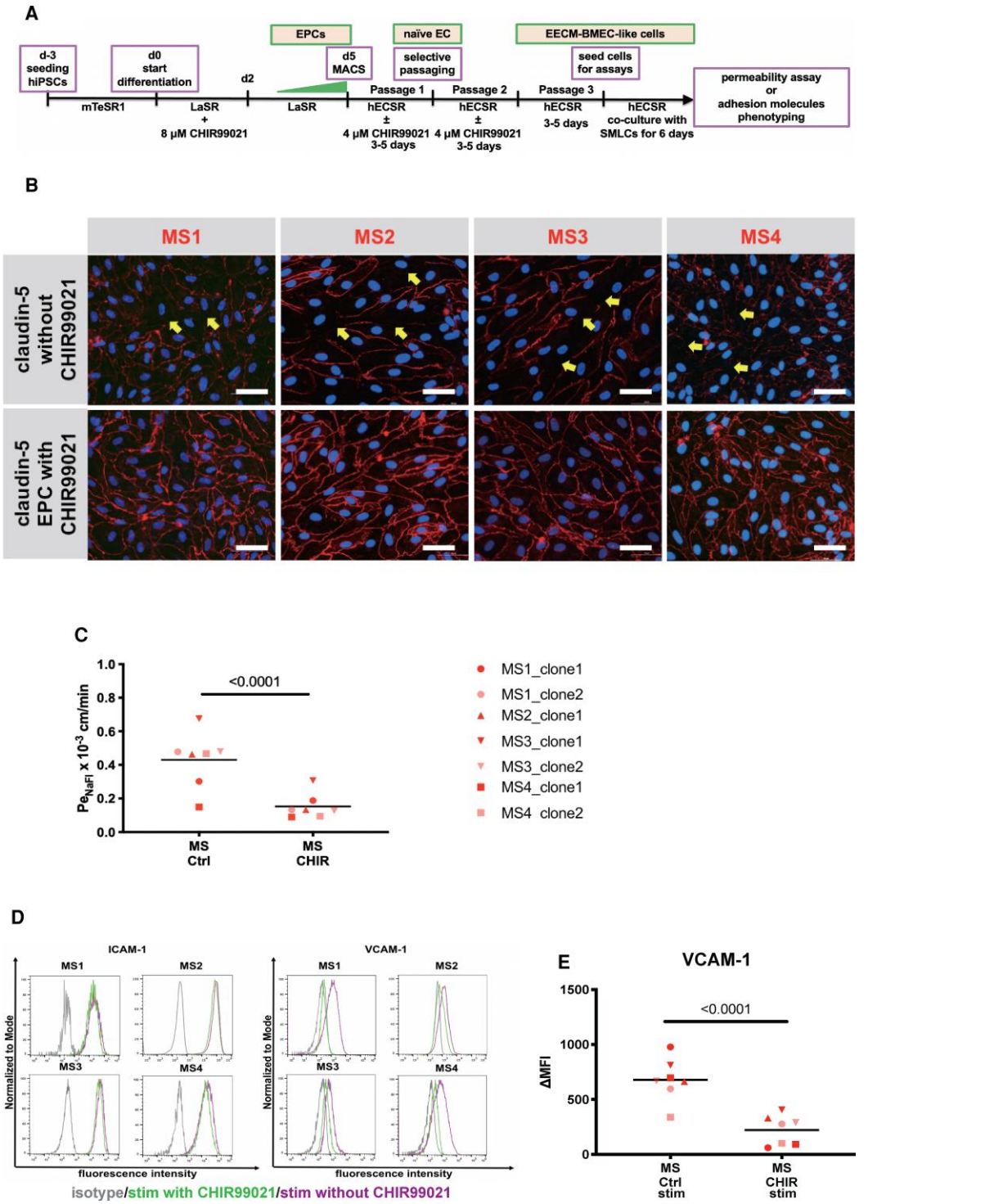

Figure 5 Pre-activation of Wnt/β-catenin signalling in MS-derived EECM-BMEC-like cells restores barrier characteristics. (**A**) Schematic representation of the activation of the Wnt/β-catenin signalling pathway in EPCs. (**B**) Immunofluorescence staining for claudin-5 (red) and nuclei (DAPI, blue) of passage 3 EECM-BMEC-like cells is shown. Representative images for clones derived from four MS patients of at least three independent experiments using three individual differentiations performed on three distinct filters are shown. Yellow arrows indicate disruptions in junctional claudin-5 staining. Scale bar = 50 μm. (**C**) Permeability of NaFl across passage 3 EECM-BMEC-like cell monolayers in the presence of absence of pre-treatment with 4 μM CHIR99021 are shown. (**D**) Cell surface staining of EECM-BMEC-like cells for the adhesion molecules ICAM-1 and VCAM-1 in the presence of absence of pre-treatment with 4 μM CHIR99021 under NS and pro-inflammatory cytokines-stimulated condition was analysed by flow cytometry. Isotype control, DMSO control and CHIR99021 treatment condition are represented in grey, red, and green lines, respectively. Representative data from Patients MS1–MS4 are shown. (**E**) The change in geometric mean (ΔMFI = MFI staining–MFI isotype) of cell surface VCAM-1 of EECM-BMEC-like cells were analysed by flow cytometry. (**C** and **E**) Bars show the mean of seven clones from four MS patients. Each symbol represents the mean of at least two independent experiments using two individual differentiations each performed in at least triplicates. Statistical analysis was performed as outlined in the 'Materials and methods' section. *P*-values are indicated in the respective figures.

and *LEF1* mRNA expression were not modified, we found mRNA expression of the canonical wnt-target gene *AXIN2* to be significantly decreased and mRNA expression of *FZD6*, previously reported as negative regulator of Wnt signalling to be significantly increased[59] in MS-derived EECM-BMEC-like cells compared to HC-derived EECM-BMEC-like cells. These data indicate that canonical Wnt/β-catenin signalling is impaired in MS-derived EECM-BMEC-like cells. Therefore, we next asked if activation of Wnt/β-catenin signalling in MS-derived EECM-BMEC-like cells would improve their barrier function. To this end, we cultured EPCs in the presence or absence of the GSK-3 inhibitor, CHIR99021, to activate Wnt/β-catenin signalling until they reached passage 3 (Fig. 5A). We investigated subcellular localization of claudin-5 in EECM-BMEC-like cells since junctional localization of claudin-5 correlates to BBB integrity in humans *in vivo* and is a known target of Wnt signalling.[60] Activation of canonical Wnt/β-catenin signalling in MS-derived EPCs resulted in improved junctional localization of claudin-5 and occludin in differentiated EECM-BMEC-like cells (Fig. 5B and Supplementary Fig. 3F). This was accompanied by reduced permeability of CHIR99021-pretreated EECM-BMEC-like cells to sodium fluorescein, reaching permeability levels comparable to HC-derived EECM-BMEC-like cells (Figs 2D and 5C, MS-derived EECM-BMEC-like cells from EPCs treated with CHIR99021 $0.147 \pm 0.081 \times 10^{-3}$ cm/min versus HC-derived EECM-BMEC-like cells $0.208 \pm 0.058 \times 10^{-3}$ cm/min). We furthermore observed that activation of Wnt/β-catenin signalling in MS-derived EPCs reduced cell surface expression of VCAM-1, but not ICAM-1 in cytokine-stimulated MS-derived EECM-BMEC-like cells (Fig. 5D and E). Thus, activation of Wnt/β-catenin signalling during the differentiation of MS-derived EECM-BMEC-like cells could restore barrier properties and reduce the inflammatory phenotype, underscoring the suitability of MS-derived EECM-BMEC-like cells for exploring therapeutic avenues for BBB stabilization and inhibition of CNS inflammation.

Discussion

The establishment of patient-sourced hiPSC-derived BMEC-like cells as *in vitro* model for the BBB has paved the way to study BBB dysfunction in a personalized fashion by providing a scalable and renewable source of BMECs from one individual. Human iPSC-derived *in vitro* models of the BBB have been established using different differentiation protocols[19,20,22,23,43] and have already proven successful to model BBB dysfunction in inheritable neurological disorders like Huntington's disease, familial Parkinson's disease, familial amyotrophic lateral sclerosis (ALS), familial Alzheimer's disease, and MCT8 deficiency *in vitro*.[24,25,27] Previous studies making use of hiPSCs from patients with sporadic ALS have proven suitable for exploring disease pathogenesis.[61] This encouraged us to establish hiPSCs from MS patients and healthy controls to explore if intrinsic defects in brain endothelial cells contribute to BBB dysfunction in MS, which may thus reveal a pathogenic process not yet fully understood.

BBB dysfunction accompanied by increased immune cell infiltration into the CNS is an early hallmark of MS pathogenesis and BBB dysfunction detected as Gd-enhancing lesions by MRI is one of the diagnostic criterions for MS. The aetiology of MS remains unknown. However, given recent discoveries that MS-associated genetic variants code for molecules related to the function of specific immune cell subsets, the disease is considered a chronic inflammatory CNS disease of autoimmune aetiology, influenced by genetic and environmental factors.[62] Immune cells from blood or CSF of MS patients have thus been extensively studied, which has increased our understanding of MS pathogenesis, leading to current development of immunomodulatory therapies for preventing MS relapse. The individual differences observed in response to MS immunomodulatory therapies combined with the variable disease course underscore that the underlying pathogenesis in MS may be much more complex than presently thought.

To this end, the GWAS studies in MS have provided little evidence for a causal contribution of CNS-resident cells in MS pathogenesis. However, this may change with increasing availability of CNS datasets pointing to the contribution of CNS-resident cells in MS pathogenesis.[63] Therefore, there is an unmet need for continued detailed phenotypic and functional analysis of disease-relevant tissues directly derived from MS patients to unravel the aetiology of MS in its entire complexity.

In this study, we show that MS-derived hiPSC-derived BMEC-like cells model BBB alterations in MS *in vitro*. Comparing MS- versus HC-derived BMEC-like cells we found that MS-derived BMEC-like cells displayed reduced barrier characteristics shown by impaired junctional integrity, reduced TEER, increased permeability to small molecular tracers and impaired efflux pump activity. These phenotypes are reflective of reports of BBB dysfunction observed in rodent models and humans.[8–11,14–16,64,65] Importantly, barrier dysfunction in MS-derived BMEC-like cells was observed using two distinct differentiation protocols, namely DMM[23] and EECM[20,43] and in BMEC-like cells from multiple hiPSC clones. Although biological sample size in our study is still limited, the observation that all MS-derived BMEC-like cells display altered barrier properties when compared to HC-derived BMEC-like cells highlights that the impaired barrier characteristics observed in MS-derived BMEC-like cells are really intrinsic to MS and are likely a result of the genetic or epigenetic profile of each individual rather than a methodological artefact. These data thus strongly support that MS patients have intrinsic alterations in their brain endothelium that lead to BBB dysfunction, which can be modelled by hiPSC-derived BMEC-like cells.

Making use of the EECM-BMEC-like cells, we further showed that impaired barrier characteristics of MS-derived BMEC-like cells were accompanied by a pro-inflammatory phenotype characterized by enhanced expression of VCAM-1 and ICAM-1 and increased immune cell interactions under static and physiological flow conditions. Making use of MS-patient derived *in vitro* BBB models, we had the unprecedented opportunity to explore how this altered BBB phenotype affects immune cell interaction in an entirely autologous fashion. Our observations underscore the active role of MS-derived EECM-BMEC-like cells in mediating the increased interaction of autologous PBMCs under static and physiological flow conditions leading to their enhanced migration across BMEC-like cells *in vitro*. MS-derived EECM-BMEC-like cells are thus a suitable model to study the molecular mechanisms leading to increased immune cell infiltration into the CNS during MS in an autologous fashion.

Having established that MS-derived BMEC-like cells allow modelling of BBB dysfunction observed in MS, we next asked if these hiPSC-derived *in vitro* BBB models are suitable to explore therapeutic approaches for restoring BBB function as potential novel treatment strategy in MS. Based on the observation that endothelial Wnt/β-catenin signalling is involved in BBB development and maturation, where Wnt/β-catenin signalling pathway stabilizes endothelial adherens junctions and tight junctions,[55–57,66,67] we asked if triggering the Wnt/β-catenin signalling pathway in MS-derived EECM-BMEC-like cells would restore barrier function. We indeed observed that activation of the Wnt/β-catenin signalling pathway

in MS-derived EECM-BMEC like cells restored their junctional integrity by improving junctional localization of claudin-5 as well as their barrier properties making them comparable to HC-derived EECM-BMEC-like cells. Our observations thus suggest that activation of the Wnt/β-catenin signalling pathway in brain endothelial cells may allow restoration of BBB function in MS. Activation of endothelial Wnt/β-catenin signalling has proven beneficial in animal models of stroke.[68,69] In the case of MS, the Wnt/β-catenin pathway was reported to be upregulated in brain endothelial cells in MS and in the mouse model EAE,[70] where its increased activity in brain endothelial cells during EAE progression was found to correlate to breakdown of the endothelial cell junctions, suggesting upregulation of Wnt/β-catenin pathway for restoring BBB function. It thus remains to be shown if the presence of pro-inflammatory factors inducing BBB dysfunction *in vivo*[62,71–76] may mask the effect of Wnt/β-catenin signalling in stabilizing BBB junctions.

In accordance with the observations in EAE *in vivo*,[70] we also observed that activation of Wnt/β-catenin signalling in MS-derived EPCs induced a quiescent immune phenotype in MS-derived EECM-BMEC-like cells with reduced expression of VCAM-1 that may result in reduced immune cell interaction. Taken together, these findings suggest that activation of endothelial Wnt/β-catenin signalling is a promising approach to restore barrier properties and a quiescent immune phenotype of the BBB in MS.

These findings are especially relevant given the fact that the current immunomodulatory treatments in MS mainly target immune cells and have limited effects on the progressive phase of MS. Therapeutic stabilization of impaired BBB function by activating Wnt/β-catenin signalling in brain endothelial cells or by other methods may thus open up entirely novel avenues for therapeutic intervention in MS by re-establishing CNS homeostasis and preventing disease progression. Consistent with this hypothesis, ectopic endothelial cell-specific expression of the tight junction sealing protein claudin-1 reduced BBB leakiness to plasma proteins during EAE resulting in amelioration of the chronic phase of the disease.[77]

Our observations thus suggests that hiPSC-derived BMEC-like cells from MS patients, and especially EECM-BMEC-like cells, model BBB dysfunction in MS with respect to junctional integrity, diffusion barrier properties, efflux pump activity, adhesion molecule phenotype, and autologous immune cell interaction. However, a shortcoming of our current study is that the matching of the MS patients and HC especially with respect to age was not ideal with the HC individuals being older than the MS patients. However, if age played a major role in determining the barrier properties of the hiPSC-derived BMEC-like cells we would have rather expected to see impaired barrier properties and an inflammatory phenotype in EECM-BMEC-like cells derived from hiPSC from the older individuals as BBB impairment is observed in healthy ageing.[78] The observation that EECM-BMEC-like cells derived from the younger MS patients displayed impaired barrier properties and an inflammatory phenotype when compared to those from the older HC-derived EECM-BMEC-like cells suggests that it is the condition of MS rather than the age of the individuals that correlates with impaired BBB properties.

Taken together, we consider hiPSC-derived BMEC-like cells to provide an unprecedented opportunity to explore the molecular mechanisms underlying BBB dysfunction in MS. Future studies comparing a higher number of sex and age matched HC and MS-patients and combining characterization of the transcriptional, phenotypic and functional profile of MS-derived EECM-BMEC-like cells compared to their HC counterparts will be necessary to identify the potential BBB dysfunction gene signatures in MS. This will set the stage for designing entirely novel therapeutic approaches that aim to stabilize BBB function in MS, bearing the hope of delaying disease onset, improving neuroprotection and preventing secondary progressive MS.

Acknowledgements

We thank David Laplaud for providing blood samples from two MS subjects enrolled in this study.

Funding

This study was funded by the SNSF (grant N° 310030_189080), the Bangerter-Rhyner Foundation and the Bern Center for Precision Medicine to B.E., the Swiss MS Society to B.E. and R.D.P.; an ECTRIMS Postdoctoral Research Exchange Fellowship, the Uehara Memorial Foundation, and JSPS Overseas Research Fellowships, and FOCS project of Yamaguchi University to H.N., and National Institutes of Health Grant NS103844 to E.V.S. and S.P.P. R.D.P. was also supported by a SNSF 320030-179531. B.D.G. was supported by the National Science Foundation Graduate Research Fellowship program under grant number 1747503 and the National Institutes of Health Biotechnology Training Program grant T32 GM008349.

Competing interests

B.E. received a grant from Biogen to study extended dosing of Natalizumab on T-cell migration across the BBB and a grant from CSL Behring to investigate the molecular underpinnings of BBB dysfunction in neurological disorders. H.N., B.D.G., S.P.P., E.V.S. and B.E. are inventors on an international patent application related to the EECM-BMEC-like cells (publication number WO/2022/072354).

Supplementary material

Supplementary material is available at *Brain* online.

References

1. Axisa PP, Hafler DA. Multiple sclerosis: genetics, biomarkers, treatments. *Curr Opin Neurol*. 2016;29:345–353.
2. International Multiple Sclerosis Genetics Consortium. Low-frequency and rare-coding variation contributes to multiple sclerosis risk. *Cell*. 2018;175:1679–1687.e7.
3. Thompson AJ, Baranzini SE, Geurts J, Hemmer B, Ciccarelli O. Multiple sclerosis. *Lancet*. 2018;391:1622–1636.
4. Kermode AG, Thompson AJ, Tofts P, *et al*. Breakdown of the blood-brain barrier precedes symptoms and other MRI signs of new lesions in multiple sclerosis. Pathogenetic and clinical implications. *Brain*. 1990;113:1477–1489.
5. Filippi M, Rovaris M, Capra R, *et al*. A multi-centre longitudinal study comparing the sensitivity of monthly MRI after standard and triple dose gadolinium-DTPA for monitoring disease activity in multiple sclerosis. Implications for phase II clinical trials. *Brain*. 1998;121:2011–2020.
6. Werring DJ, Brassat D, Droogan AG, *et al*. The pathogenesis of lesions and normal-appearing white matter changes in multiple sclerosis: a serial diffusion MRI study. *Brain*. 2000;123:1667–1676.

7. Goodkin DE, Rooney WD, Sloan R, *et al*. A serial study of new MS lesions and the white matter from which they arise. *Neurology*. 1998;51:1689–1697.
8. Plumb J, McQuaid S, Mirakhur M, Kirk J. Abnormal endothelial tight junctions in active lesions and normal-appearing white matter in multiple sclerosis. *Brain Pathol*. 2002;12:154–169.
9. Kirk J, Plumb J, Mirakhur M, McQuaid S. Tight junctional abnormality in multiple sclerosis white matter affects all calibres of vessel and is associated with blood-brain barrier leakage and active demyelination. *J Pathol*. 2003;201:319–327.
10. Leech S, Kirk J, Plumb J, McQuaid S. Persistent endothelial abnormalities and blood-brain barrier leak in primary and secondary progressive multiple sclerosis. *Neuropathol Appl Neurobiol*. 2007;33:86–98.
11. Alvarez JI, Cayrol R, Prat A. Disruption of central nervous system barriers in multiple sclerosis. *Biochim Biophys Acta*. 2011;1812: 252–264.
12. Alvarez JI, Saint-Laurent O, Godschalk A, *et al*. Focal disturbances in the blood-brain barrier are associated with formation of neuroinflammatory lesions. *Neurobiol Dis*. 2015;74:14–24.
13. Vos CM, Geurts JJ, Montagne L, *et al*. Blood-brain barrier alterations in both focal and diffuse abnormalities on postmortem MRI in multiple sclerosis. *Neurobiol Dis*. 2005;20:953–960.
14. Kooij G, van Horssen J, de Lange EC, *et al*. T lymphocytes impair P-glycoprotein function during neuroinflammation. *J Autoimmun*. 2010;34:416–425.
15. Sobel RA, Mitchell ME, Fondren G. Intercellular adhesion molecule-1 (ICAM-1) in cellular immune reactions in the human central nervous system. *Am J Pathol*. 1990;136:1309–1316.
16. Cayrol R, Wosik K, Berard JL, *et al*. Activated leukocyte cell adhesion molecule promotes leukocyte trafficking into the central nervous system. *Nat Immunol*. 2008;9:137–145.
17. Minten C, Alt C, Gentner M, *et al*. DARC shuttles inflammatory chemokines across the blood-brain barrier during autoimmune central nervous system inflammation. *Brain*. 2014;137:1454–1469.
18. Klotz L, Kuzmanov I, Hucke S, *et al*. B7-H1 shapes T-cell-mediated brain endothelial cell dysfunction and regional encephalitogenicity in spontaneous CNS autoimmunity. *Proc Natl Acad Sci USA*. 2016;113:E6182–E6191.
19. Lippmann ES, Azarin SM, Kay JE, *et al*. Derivation of blood-brain barrier endothelial cells from human pluripotent stem cells. *Nat Biotechnol*. 2012;30:783–791.
20. Nishihara H, Gastfriend BD, Soldati S, *et al*. Advancing human induced pluripotent stem cell-derived blood-brain barrier models for studying immune cell interactions. *FASEB J*. 2020;34:16693–16715.
21. Praça C, Rosa SC, Sevin E, Cecchelli R, Dehouck MP, Ferreira LS. Derivation of brain capillary-like endothelial cells from human pluripotent stem cell-derived endothelial progenitor cells. *Stem Cell Rep*. 2019;13:599–611.
22. Stebbins MJ, Wilson HK, Canfield SG, Qian T, Palecek SP, Shusta EV. Differentiation and characterization of human pluripotent stem cell-derived brain microvascular endothelial cells. *Methods*. 2016;101:93–102.
23. Qian T, Maguire SE, Canfield SG, *et al*. Directed differentiation of human pluripotent stem cells to blood-brain barrier endothelial cells. *Sci Adv*. 2017;3:e1701679.
24. Lim RG, Quan C, Reyes-Ortiz AM, *et al*. Huntington's disease iPSC-derived brain microvascular endothelial cells reveal WNT-mediated angiogenic and blood-brain barrier deficits. *Cell Rep*. 2017;19:1365–1377.
25. Vatine GD, Al-Ahmad A, Barriga BK, *et al*. Modeling psychomotor retardation using iPSCs from MCT8-deficient patients indicates a prominent role for the blood-brain barrier. *Cell Stem Cell*. 2017;20:831–843.e5.
26. Vatine GD, Barrile R, Workman MJ, *et al*. Human iPSC-derived blood-brain barrier chips enable disease modeling and personalized medicine applications. *Cell Stem Cell*. 2019;24: 995–1005.e6.
27. Katt ME, Mayo LN, Ellis SE, *et al*. The role of mutations associated with familial neurodegenerative disorders on blood-brain barrier function in an iPSC model. *Fluids Barriers CNS*. 2019;16:20.
28. Oikari LE, Pandit R, Stewart R, *et al*. Altered brain endothelial cell phenotype from a familial alzheimer mutation and its potential implications for amyloid clearance and drug delivery. *Stem Cell Rep*. 2020;14:924–939.
29. Nicaise AM, Banda E, Guzzo RM, *et al*. iPS-derived neural progenitor cells from PPMS patients reveal defect in myelin injury response. *Exp Neurol*. 2017;288:114–121.
30. Song B, Sun G, Herszfeld D, *et al*. Neural differentiation of patient specific iPS cells as a novel approach to study the pathophysiology of multiple sclerosis. *Stem Cell Res*. 2012;8:259–273.
31. Martínez-Larrosa J, Matute-Blanch C, Montalban X, Comabella M. Modelling multiple sclerosis using induced pluripotent stem cells. *J Neuroimmunol*. 2020;349:577425.
32. Perriot S, Mathias A, Perriard G, *et al*. Human induced pluripotent stem cell-derived astrocytes are differentially activated by multiple sclerosis-associated cytokines. *Stem Cell Rep*. 2018; 11:1199–1210.
33. Douvaras P, Wang J, Zimmer M, *et al*. Efficient generation of myelinating oligodendrocytes from primary progressive multiple sclerosis patients by induced pluripotent stem cells. *Stem Cell Rep*. 2014;3:250–259.
34. García-León JA, Kumar M, Boon R, *et al*. SOX10 single transcription factor-based fast and efficient generation of oligodendrocytes from human pluripotent stem cells. *Stem Cell Rep*. 2018; 10:655–672.
35. Ponath G, Lincoln MR, Levine-Ritterman M, *et al*. Enhanced astrocyte responses are driven by a genetic risk allele associated with multiple sclerosis. *Nat Commun*. 2018;9:5337.
36. Nicaise AM, Wagstaff LJ, Willis CM, *et al*. Cellular senescence in progenitor cells contributes to diminished remyelination potential in progressive multiple sclerosis. *Proc Natl Acad Sci USA*. 2019;116:9030–9039.
37. Pantoja IEM, Smith MD, Rajbhandari L, *et al*. iPSCs from people with MS can differentiate into oligodendrocytes in a homeostatic but not an inflammatory milieu. *PLoS One*. 2020; 15:e0233980.
38. Sullivan S, Stacey GN, Akazawa C, *et al*. Quality control guidelines for clinical-grade human induced pluripotent stem cell lines. *Regen Med*. 2018;13:859–866.
39. Engen SA, Valen Rukke H, Becattini S, *et al*. The oral commensal Streptococcus mitis shows a mixed memory Th cell signature that is similar to and cross-reactive with Streptococcus pneumoniae. *PLoS One*. 2014;9:e104306.
40. Sallusto F, Schaerli P, Loetscher P, *et al*. Rapid and coordinated switch in chemokine receptor expression during dendritic cell maturation. *Eur J Immunol*. 1998;28:2760–2769.
41. Wimmer I, Tietz S, Nishihara H, *et al*. PECAM-1 stabilizes blood-brain barrier integrity and favors paracellular T-cell diapedesis across the blood-brain barrier during neuroinflammation. original research. *Front Immunol*. 2019;10:711.
42. Jilek S, Schluep M, Meylan P, *et al*. Strong EBV-specific CD8+ T-cell response in patients with early multiple sclerosis. *Brain*. 2008;131:1712–1721.
43. Nishihara H, Gastfriend BD, Kasap P, Palecek SP, Shusta EV, Engelhardt B. Differentiation of human pluripotent stem cells to brain microvascular endothelial cell-like cells suitable to study immune cell interactions. *STAR Protoc*. 2021;2:100563.

44. Nishihara H, Soldati S, Mossu A, *et al*. Human CD4(+) T cell subsets differ in their abilities to cross endothelial and epithelial brain barriers in vitro. *Fluids Barriers CNS*. 2020;17:3.
45. Mossu A, Rosito M, Khire T, *et al*. A silicon nanomembrane platform for the visualization of immune cell trafficking across the human blood-brain barrier under flow. *J Cere Blood Flow Metab*. 2018;39:395–410.
46. Workman MJ, Svendsen CN. Recent advances in human iPSC-derived models of the blood-brain barrier. *Fluids Barriers CNS*. 2020;17:30.
47. Lippmann ES, Azarin SM, Palecek SP, Shusta EV. Commentary on human pluripotent stem cell-based blood-brain barrier models. *Fluids Barriers CNS*. 2020;17:64.
48. Lu TM, Houghton S, Magdeldin T, *et al*. Pluripotent stem cell-derived epithelium misidentified as brain microvascular endothelium requires ETS factors to acquire vascular fate. *Proc Natl Acad Sci USA*. 2021;118:e2016950118.
49. Abadier M, Haghayegh Jahromi N, Cardoso Alves L, *et al*. Cell surface levels of endothelial ICAM-1 influence the transcellular or paracellular T-cell diapedesis across the blood-brain barrier. *Eur J Immunol*. 2015;45:1043–1058.
50. Nishihara H, Engelhardt B. Brain barriers and multiple sclerosis: Novel treatment approaches from a brain barriers perspective. In: *Handbook of Experimental Pharmacology*. Springer; 2020:1–35.
51. Kebir H, Ifergan I, Alvarez JI, *et al*. Preferential recruitment of interferon-gamma-expressing TH17 cells in multiple sclerosis. *Ann Neurol*. 2009;66:390–402.
52. van Langelaar J, van der Vuurst de Vries RM, Janssen M, *et al*. T helper 17.1 cells associate with multiple sclerosis disease activity: perspectives for early intervention. *Brain*. 2018;141:1334–1349.
53. Jelcic I, Al Nimer F, Wang J, *et al*. Memory B cells activate brain-homing, autoreactive CD4(+) T cells in multiple sclerosis. *Cell*. 2018;175:85–100.e23.
54. Mathias A, Perriot S, Canales M, *et al*. Impaired T-cell migration to the CNS under fingolimod and dimethyl fumarate. *Neurol Neuroimmunol Neuroinflamm*. 2017;4:e401.
55. Zhou Y, Wang Y, Tischfield M, *et al*. Canonical WNT signaling components in vascular development and barrier formation. *J Clin Invest*. 2014;124:3825–3846.
56. Stenman JM, Rajagopal J, Carroll TJ, Ishibashi M, McMahon J, McMahon AP. Canonical Wnt signaling regulates organ-specific assembly and differentiation of CNS vasculature. *Science*. 2008;322:1247–1250.
57. Daneman R, Agalliu D, Zhou L, Kuhnert F, Kuo CJ, Barres BA. Wnt/beta-catenin signaling is required for CNS, but not non-CNS, angiogenesis. *Proc Natl Acad Sci USA*. 2009;106:641–646.
58. Gastfriend BD, Nishihara H, Foreman KL, *et al*. Wnt signaling mediates acquisition of blood-brain barrier properties in naïve endothelium derived from human pluripotent stem cells. *eLife*. 2021;10:e70992.
59. Golan T, Yaniv A, Bafico A, Liu G, Gazit A. The human frizzled 6 (HFz6) acts as a negative regulator of the canonical Wnt. beta-catenin signaling cascade. *J Biol Chem*. 2004;279:14879–14888.
60. Doherty CP, O'Keefe E, Wallace E, *et al*. Blood-brain barrier dysfunction as a hallmark pathology in chronic traumatic encephalopathy. *J Neuropathol Exp Neurol*. 2016;75:656–662.
61. Fujimori K, Ishikawa M, Otomo A, *et al*. Modeling sporadic ALS in iPSC-derived motor neurons identifies a potential therapeutic agent. *Nat Med*. 2018;24:1579–1589.
62. Baecher-Allan C, Kaskow BJ, Weiner HL. Multiple sclerosis: Mechanisms and immunotherapy. *Neuron*. 2018;97:742–768.
63. Cotsapas C, Mitrovic M. Genome-wide association studies of multiple sclerosis. *Clin Transl Immunol*. 2018;7:e1018.
64. Alvarez JI, Kebir H, Cheslow L, *et al*. JAML mediates monocyte and CD8T cell migration across the brain endothelium. *Ann Clin Transl Neurol*. 2015;2:1032–1037.
65. Bennett J, Basivireddy J, Kollar A, *et al*. Blood-brain barrier disruption and enhanced vascular permeability in the multiple sclerosis model EAE. *J Neuroimmunol*. 2010;229:180–191.
66. Liebner S, Corada M, Bangsow T, *et al*. Wnt/beta-catenin signaling controls development of the blood-brain barrier. *J Biol*. 2008;183:409–417.
67. Tran KA, Zhang X, Predescu D, *et al*. Endothelial β-catenin signaling is required for maintaining adult blood-brain barrier integrity and central nervous system homeostasis. *Circulation*. 2016;133:177–186.
68. LeBlanc NJ, Menet R, Picard K, Parent G, Tremblay M, ElAli A. Canonical Wnt pathway maintains blood-brain barrier integrity upon ischemic stroke and its activation ameliorates tissue plasminogen activator therapy. *Mol Neurobiol*. 2019;56:6521–6538.
69. Song S, Huang H, Guan X, *et al*. Activation of endothelial Wnt/β-catenin signaling by protective astrocytes repairs BBB damage in ischemic stroke. *Prog Neurobiol*. 2021;199:101963.
70. Lengfeld JE, Lutz SE, Smith JR, *et al*. Endothelial Wnt/β-catenin signaling reduces immune cell infiltration in multiple sclerosis. *Proc Natl Acad Sci USA*. 2017;114:E1168–E1177.
71. Hojati Z. Molecular genetic and epigenetic basis of multiple sclerosis. *Adv Exp Med Biol*. 2017;958:65–90.
72. Becher B, Spath S, Goverman J. Cytokine networks in neuroinflammation. *Nat Rev Immunol*. 2017;17:49–59.
73. Brosnan CF, Cannella B, Battistini L, Raine CS. Cytokine localization in multiple sclerosis lesions: correlation with adhesion molecule expression and reactive nitrogen species. *Neurology*. 1995;45:S16–S21.
74. Perriard G, Mathias A, Enz L, *et al*. Interleukin-22 is increased in multiple sclerosis patients and targets astrocytes. *J Neuroinflammation*. 2015;12:119.
75. Yong VW, Zabad RK, Agrawal S, Goncalves Dasilva A, Metz LM. Elevation of matrix metalloproteinases (MMPs) in multiple sclerosis and impact of immunomodulators. *J Neurol Sci*. 2007;259:79–84.
76. Kebir H, Kreymborg K, Ifergan I, *et al*. Human TH17 lymphocytes promote blood-brain barrier disruption and central nervous system inflammation. *Nat Med*. 2007;13:1173–1175.
77. Pfeiffer F, Schafer J, Lyck R, *et al*. Claudin-1 induced sealing of blood-brain barrier tight junctions ameliorates chronic experimental autoimmune encephalomyelitis. *Acta Neuropathol*. 2011;122:601–614.
78. Montagne AB, Sweeney SR, MD *et al*. Blood-brain barrier breakdown in the aging human hippocampus. *Neuron*. 2015;85:296–302.